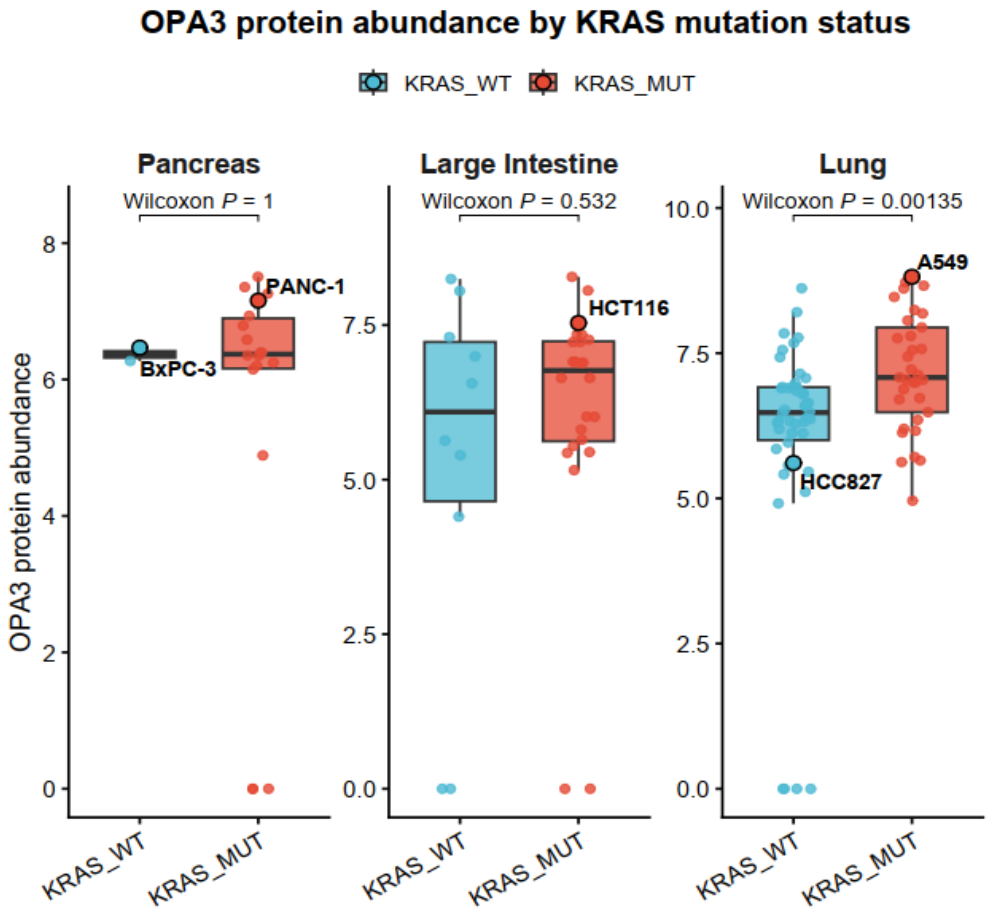
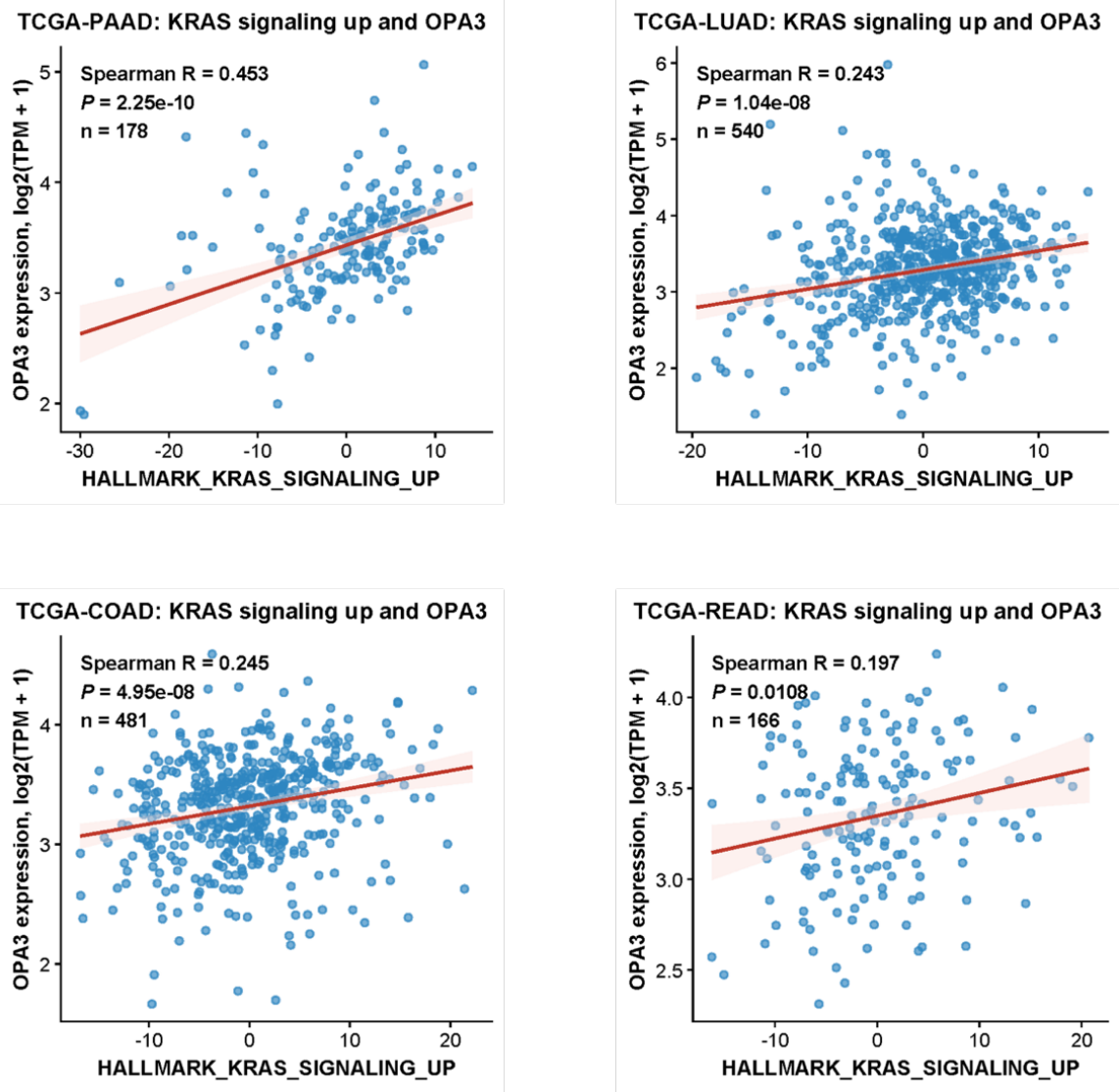
Supplementary Materials

Supplementary Figure S1 compares OPA3 protein abundance according to KRAS mutation status in cancer cell lines.



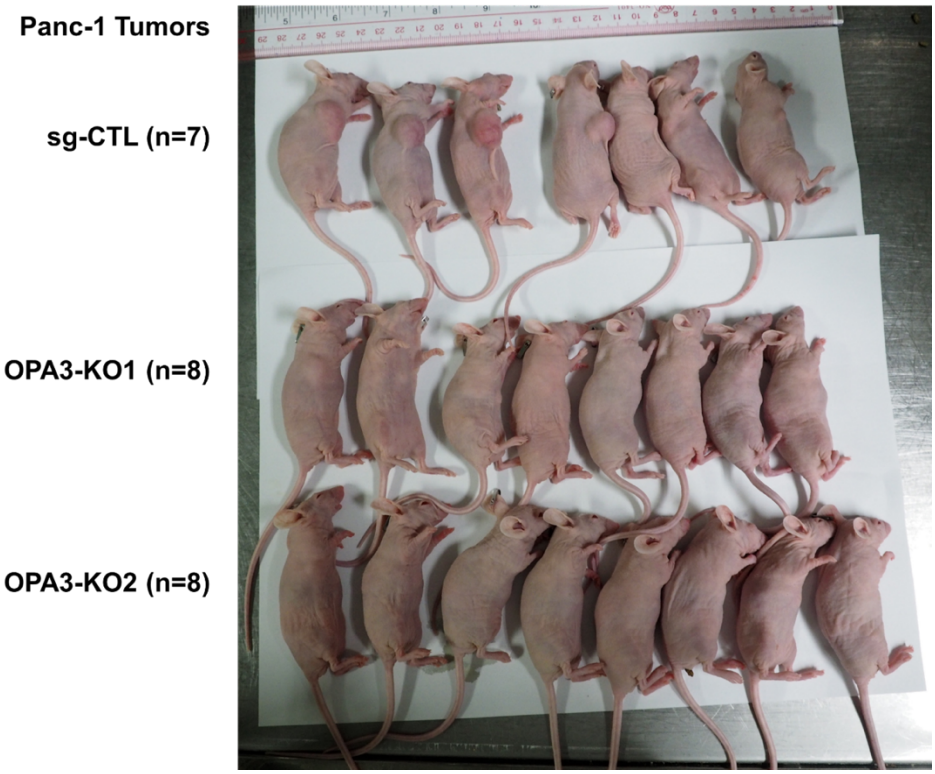
Suppl Figure S1. CCLE proteomic analysis. *OPA3 protein levels were compared in pancreatic (KRAS-WT, n=2; KRAS-MUT, n=18), colon (KRAS-WT, n=10; KRAS-MUT, n=24), and lung (KRAS-WT, n=46; KRAS-MUT, n=33) KRAS-mutant and KRAS-wild-type cancer cell lines. Statistics: Wilcoxon rank-sum test.* ***Abbreviations:*** *CCLE, Cancer Cell Line Encyclopedia; KRAS, Kirsten rat sarcoma viral oncogene homolog; MUT, mutant; OPA3, optic atrophy protein 3; WT, wild-type.*

Supplementary Figure S2 examines associations between KRAS signaling activity and OPA3 expression across selected cancer types.



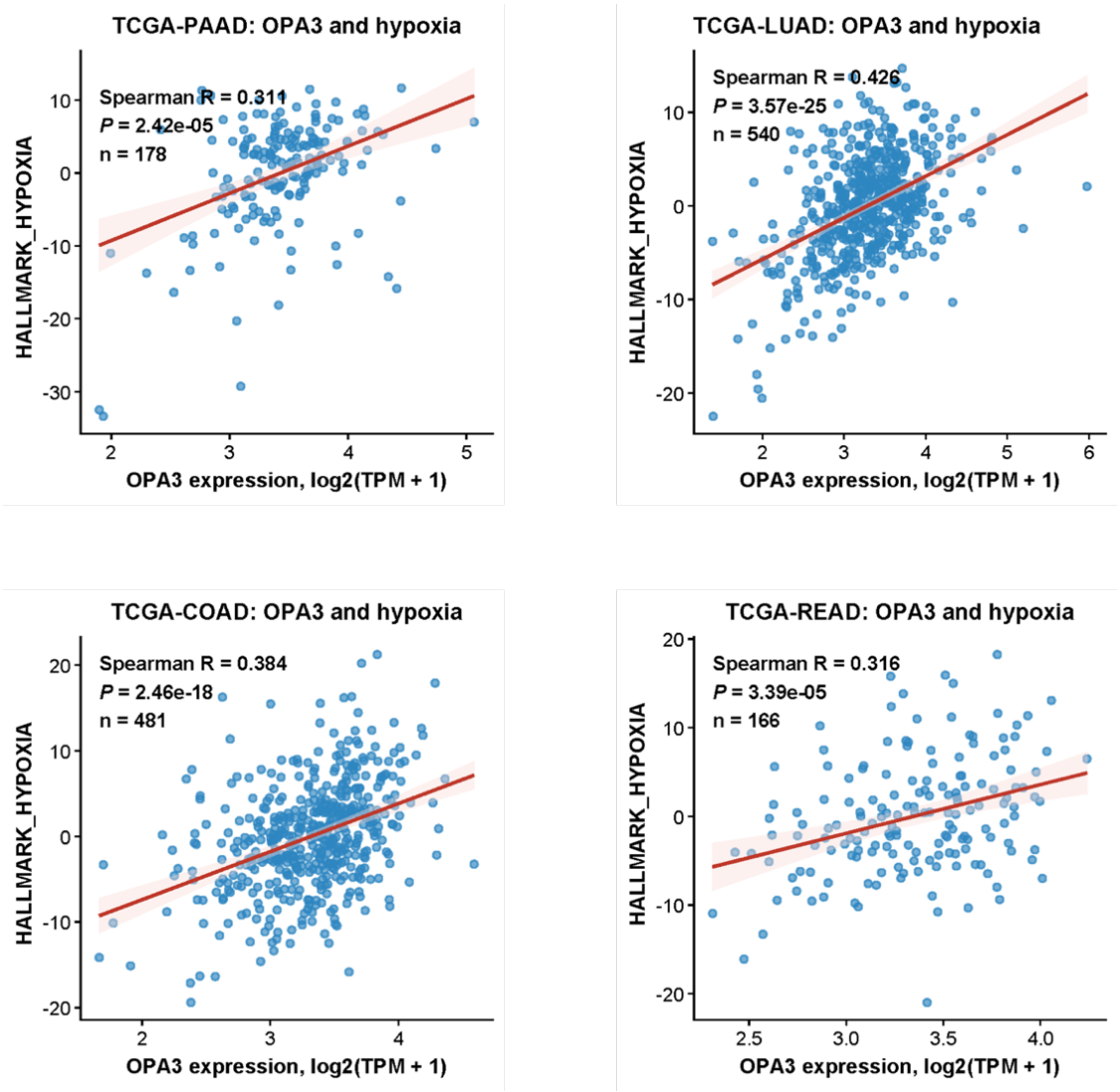
Suppl Figure S2. Correlation between KRAS signaling and OPA3 expression. *Correlation between KRAS signaling activity and OPA3 mRNA levels was quantified in pancreatic (PAAD), lung (LUAD), colon (COAD), and rectal (READ) cancers using TCGA analysis. Statistics: Spearman rank test.* ***Abbreviations:*** *COAD, colon adenocarcinoma; KRAS, Kirsten rat sarcoma viral oncogene homolog; LUAD, lung adenocarcinoma; OPA3, optic atrophy protein 3; PAAD, pancreatic adenocarcinoma; READ, rectum adenocarcinoma; TCGA, The Cancer Genome Atlas.*

Supplementary Figure S3 presents photographs of mice bearing control or OPA3-knockout pancreatic tumors



Suppl Figure S3. Photograph of tumor-bearing mice. *Nude BALB/c mice were inoculated with control or OPA3-KO PANC-1 cancer cells.* ***Abbreviations****: KO, knockout; OPA3, optic atrophy protein 3; sg-CTL, control single-guide RNA group.*

Supplementary Figure S4 illustrates associations between OPA3 expression and hypoxia-related transcriptional activity.



Suppl Figure S4. Correlation between hypoxia-related pathways and OPA3 expression. *Correlation between hypoxia pathway activity and OPA3 mRNA levels was quantified in pancreatic (PAAD), lung (LUAD), colon (COAD), and rectal (READ) cancers using TCGA analysis. Statistics: Spearman rank test.* ***Abbreviations:*** *COAD, colon adenocarcinoma; LUAD, lung adenocarcinoma; OPA3, optic atrophy protein 3; PAAD, pancreatic adenocarcinoma; READ, rectal adenocarcinoma; TCGA, The Cancer Genome Atlas.*

Supplementary Table S1 summarizes pan-cancer OPA3 expression patterns.

Suppl Table S1

Cancer types	Tumor (n)	Tumor (median)	Normal (n)	Normal (median)	t-statistic	limma FDR
OPA3 **expression upregulated in tumor tissues**						
SKCM	469	2,98	558	2,17	31,518	5,35E-153

PAAD	179	2,54	171	1,3	27,93	6,90E-91
ESCA	182	3,29	286	2,3	24,692	1,10E-86
STAD	414	3,18	211	2,01	23,626	1,32E-88
BRCA	1099	2,58	292	2,2	11,882	4,44E-31
GBM	166	2,75	110	2,19	10,442	1,05E-21
LGG	523	2,33	209	2,08	10,423	8,28E-24
LIHC	371	2,22	160	1,79	10,244	1,37E-22
OV	427	2,52	88	1,82	8,062	5,32E-15
LUSC	498	2,64	338	2,48	7,34	5,08E-13
COAD	290	2,54	349	2,27	7,293	9,06E-13
THCA	512	2,7	338	2,51	6,856	1,36E-11
SARC	262	2,6	398	2,37	6,703	4,38E-11
CHOL	36	2,78	9	1,66	6,7	3,50E-08
LAML	173	3,62	70	3,17	6,697	1,49E-10
KICH	66	3,52	53	2,94	5,862	4,31E-08
HNSC	520	2,78	44	2,4	5,792	1,16E-08
CESC	306	2,74	13	2,16	4,997	9,66E-07
READ	93	2,44	151	2,21	4,57	7,77E-06
ACC	77	3,13	128	2,68	3,986	9,36E-05
PRAD	496	2,45	152	2,34	2,891	0,00396
UCS	57	2,41	78	2,31	1,984	0,0493
Non-significant comparisons of *OPA3* expression between tumor and normal tissues						
KIRP	289	2,95	60	3,12	1,331	0,184
BLCA	407	2,55	28	2,49	0,736	0,462
LUAD	515	2,43	347	2,49	0,609	0,543
PCPG	182	3,08	3	2,67	0,497	0,62
UCEC	181	2,27	101	2,31	-0,006	0,995
THYM	119	2,63	2	2,69	-0,149	0,882
KIRC	531	2,9	100	3,07	-0,887	0,375
***OPA3* expression downregulated in tumor tissues**						
TGCT	154	2,62	165	3,65	-19,084	1,35E-54
DLBC	47	2,64	107	3,34	-9,806	6,79E-18

Table S1. OPA3 expression in tumor samples. *OPA3 mRNA levels in tumor tissues and corresponding normal tissues were analyzed using GEPIA based on TCGA and GTEx transcriptomic data (listed by t-statistic values; cfr.* ***Fig. 1A****). The number of samples, median expression values, t-statistics, and P-values are provided for each cancer type.* ***Abbreviations:*** *ACC, adrenocortical carcinoma; BLCA, bladder urothelial carcinoma; BRCA, breast invasive carcinoma; CESC, cervical squamous cell carcinoma and endocervical adenocarcinoma; CHOL, cholangiocarcinoma; COAD, colon adenocarcinoma; DLBC, diffuse large B-cell lymphoma;*

ESCA, esophageal carcinoma; FDR, false discovery rate; GBM, glioblastoma multiforme; GEPIA, Gene Expression Profiling Interactive Analysis; GTEx, Genotype-Tissue Expression; HNSC, head and neck squamous cell carcinoma; KICH, kidney chromophobe; KIRC, kidney renal clear cell carcinoma; KIRP, kidney renal papillary cell carcinoma; LAML, acute myeloid leukemia; LGG, brain lower-grade glioma; LIHC, liver hepatocellular carcinoma; LUAD, lung adenocarcinoma; LUSC, lung squamous cell carcinoma; OPA3, optic atrophy 3; OV, ovarian serous cystadenocarcinoma; PAAD, pancreatic adenocarcinoma; PCPG, pheochromocytoma and paraganglioma; PRAD, prostate adenocarcinoma; READ, rectum adenocarcinoma; SARC, sarcoma; SKCM, skin cutaneous melanoma; STAD, stomach adenocarcinoma; TCGA, The Cancer Genome Atlas; TGCT, testicular germ cell tumors; THCA, thyroid carcinoma; THYM, thymoma; UCEC, uterine corpus endometrial carcinoma; UCS, uterine carcinosarcoma.

Detailed description of bioinformatics

Public transcriptomic, proteomic, and spatial transcriptomic datasets were analyzed to evaluate OPA3 expression, its association with KRAS mutation status, and its relationship with KRAS- and hypoxia-related transcriptional programs. For the pan-cancer tumor-normal comparison shown in Figure 1A, *OPA3* mRNA expression across cancer types was analyzed using Gene Expression Profiling Interactive Analysis (GEPIA). GEPIA integrates RNA-seq expression profiles from The Cancer Genome Atlas (TCGA) and the Genotype-Tissue Expression (GTEx) project and provides tumor-normal expression comparisons based on log2 (TPM + 1)-transformed data. *OPA3 expression was compared between tumor and normal tissue samples across cancer types using the GEPIA differential expression module, incorporating TCGA and GTEx data as applicable*. Cancer types were ranked according to the magnitude and direction of tumor-normal differences, and cancer types with statistically significant *OPA3* upregulation or downregulation were highlighted.

To assess the association between *OPA3* expression and KRAS mutation status, TCGA pancreatic adenocarcinoma (PAAD), lung adenocarcinoma (LUAD), colon adenocarcinoma (COAD), and rectum adenocarcinoma (READ) cohorts were analyzed. Samples with available RNA-seq expression and somatic mutation data were retained. Tumors harboring non-synonymous KRAS mutations were classified as KRAS-mutant, whereas tumors without KRAS mutations were classified as KRAS-wild-type.

For cell-line proteomic validation, quantitative proteomic data from the Cancer Cell Line Encyclopedia (CCLE) were analyzed. OPA3 protein abundance values were extracted and integrated with CCLE/DepMap lineage annotations and KRAS mutation status. Pancreatic, colorectal, and lung cancer cell lines with available OPA3 protein abundance and KRAS mutation annotation were included. KRAS signaling and hypoxia-related transcriptional activities were evaluated using the Molecular Signatures Database Hallmark gene sets, including HALLMARK_KRAS_SIGNALING_UP and HALLMARK_HYPOXIA. For each TCGA tumor sample, pathway activity scores were calculated from log2 (TPM + 1)-transformed expression matrices using single-sample gene set enrichment analysis.

Publicly available 10x Genomics Visium spatial transcriptomic data from human pancreatic tissues were retrieved from the NCBI Gene Expression Omnibus (GEO; accession GSE327056) and analyzed using Python. Four samples were included: adjacent tumor tissue (GSM9647219), pancreatic cancer tissue (GSM9647220), tumor stroma (GSM9647221), and normal pancreatic tissue (GSM9647222). For each sample, the filtered feature-barcode matrix was loaded using Scanpy with gene symbols as feature names. Spatial information was reconstructed from the corresponding Visium spatial files, including tissue position files, scale factor files, and hematoxylin and eosin images. Spot coordinates were aligned with expression barcodes and stored as full-resolution spatial coordinates. Raw count matrices were first preserved and then normalized to 10,000 counts per spot, followed by log1p transformation.

To reduce sparsity and improve visualization of spatial gene expression, MAGIC imputation was performed separately for each sample using all genes, with k-nearest neighbors set to 5, decay set to 1, an automatically selected diffusion time, and the exact solver. The resulting imputed expression matrix was stored as the MAGIC expression layer and used for downstream visualization and statistical analysis. *OPA3* and *HIF1A* expression values were extracted from the MAGIC expression layer for each Visium spot. Spatial expression maps were generated by plotting MAGIC-imputed expression values on the original Visium spatial coordinates, using a common color scale across samples for each gene. H&E images were displayed to show the histological context of each tissue section. For quantitative comparisons among tissue groups, spot-level *OPA3* and *HIF1A* MAGIC expression values were combined across the four samples and grouped according to histological annotation.

To evaluate the spatial association between *OPA3* and *HIF1A*, paired spot-level MAGIC expression values of OPA3 and HIF1A were extracted from all four samples. Statistical comparisons and correlation analyses were performed at the Visium capture-spot level using MAGIC-imputed expression values. Because the four tissue categories were represented by individual tissue sections, capture spots were treated as observational units rather than independent biological replicates. Accordingly, spot-level P-values were interpreted as descriptive, exploratory measures of within-dataset differences and associations rather than evidence of reproducibility across independent biological specimens.